

Article

Field-Measurement of Surface Wind and Sediment Transport Patterns in a Coastal Dune Environment, Case Study of Cala Tirant (Menorca, Spain)

Miquel Mir-Gual ^{1,*}, Guillem X. Pons ¹, Irene Delgado-Fernández ² and Thomas A. G. Smyth ³

¹ Department of Geography, University of the Balearic Islands, 07122 Palma, Spain; guillemx.pons@uib.es

² Department of Earth Sciences, University of Cadiz, 11003 Cadiz, Spain; irene.delgado@uca.es

³ Department of Physical and Life Sciences, University of Huddersfield, Huddersfield HD1 3DH, UK; t.ag.smyth@hud.ac.uk

* Correspondence: mirgual@gmail.com

Abstract: Blowouts are integral features of coastal dune fields. Their presence enhances both geomorphological and ecological diversity and enables the movement of sand by wind. Their role as a ‘transport corridor’ may be, however, considered negative from a coastal management perspective in heavily touristic areas, where the existence of blowouts close to the foredune can enhance the loss of sediment from the beach. This paper investigated the relationship between airflow dynamics and patterns of sediment transport from the beach to established dunes through a trough blowout located on the foredune. Seven three-cup anemometers were used to measure wind speed and direction over a 24 h sampling period at a frequency of 1 min under onshore (parallel to the blowout axis) medium and high wind speeds (max of 17.9 ms⁻¹). To measure sediment transport, a total of 12 vertical sand traps were located at three positions along the length of the deflation basin. The results indicated that small amounts of sediments went into the blowout from the beach and that the highest rates of sediment remobilization took place within the deflation basin. These results highlight two processes: (a) flow channelization induced by the blowout topography caused an increase in wind speed and sediment transport toward the depositional lobe, and (b) the presence of embryo dunes and herbaceous vegetation at the beach–blowout boundary effectively reduced the amount of sediment transport from the beach to the landform. The results confirmed the significant role that vegetation plays in controlling sediment movement and conserving the beach–dune system.

Keywords: blowout; aeolian dynamics; sediment transport; dune system; erosion; management



Citation: Mir-Gual, M.; Pons, G.X.; Delgado-Fernández, I.; Smyth, T.A.G. Field-Measurement of Surface Wind and Sediment Transport Patterns in a Coastal Dune Environment, Case Study of Cala Tirant (Menorca, Spain). *J. Mar. Sci. Eng.* **2023**, *11*, 2361. <https://doi.org/10.3390/jmse11122361>

Academic Editors: Germán Flor-Blanco, Mouncef Sedrati and France Floc'h

Received: 20 November 2023
Revised: 5 December 2023
Accepted: 12 December 2023
Published: 14 December 2023



Copyright: © 2023 by the authors. Licensee MDPI, Basel, Switzerland. This article is an open access article distributed under the terms and conditions of the Creative Commons Attribution (CC BY) license (<https://creativecommons.org/licenses/by/4.0/>).

1. Introduction

There are many definitions of blowouts based on their occurrence and physical characterization [1–7]. In general, blowouts are defined as saucer- or trough-shaped depressions or hollows formed by wind erosion on a pre-existing sand deposit [8]. The depositional lobe (downwind sand accumulation) is generally considered part of the blowout, e.g., [7,9,10]. Blowouts have been classified according to their shape and physical features. Smith [11] and Ritchie [12] defined four types of blowouts: cigar-shaped, v-shaped, scooped hollow, and cauldron corridor, whereas Cooper [13] and Hesp [2,8] suggested only two, namely trough and saucer blowouts. More recently, Mir-Gual et al. [7] carried out a preliminary classification of blowouts in calcareous sands, taking into account their shape and structure, inner morphometry, and topography, and they included some additional forms, such as mixed blowouts.

Blowouts may develop naturally during a phase of aridity when the vegetation that holds the dune together deteriorates, resulting in the mobilization of wind-blown sand. Dune erosion can also be initiated by strong winds that transport sediment, often associated with increasing storminess. Blowouts also form when the outer margin of vegetated coastal

dunes is cut away by the sea during a storm, leaving an unvegetated cliff of loose sand exposed to onshore wind action [14]. When considering the origin and evolution of blowouts, several factors must be taken into account. Bate and Ferguson [3] postulated that blowouts can be formed by various processes of natural or anthropogenic disturbance that facilitate the penetration of strong winds onto the exposed dune surface. Once initiated, their further development will depend on the location, type, height, and length of the dune [15], the vegetation cover type and density [7,16,17], the strength and direction of local surface winds [18], the orientation of the dune front to the main wind direction [19], the strength and recurrence of storm waves inundating the emerged beach and foredune strip, the local topography, and the erosion caused by surface runoff [8]. In addition to such natural factors, the creation and expansion of blowouts are often related to human pressure [3] and ineffective management measures [20].

The deflation of blowout sediment can constitute a source of sand supply to inland dunes [21]. In extreme cases, blowout expansion and coalescence can lead to vast deflation and the migration of entire dune fields [22,23]. The evolution of a simple blowout can hence generate more complex structures over time, including the formation of large degraded areas [7].

Much research has been conducted concerning the effect of wind dynamics on blowout initiation and evolution. Langsberg and Riley [24] carried out one of the first studies of wind flow within a blowout. Both airflow and the role of vegetation have been subsequently studied by many aeolian researchers [2,4,6,22,25–31]. It has not been until recently, however, that technical and modeling advances have allowed for the detailed exploration of wind characteristics in a range of dune blowout forms. The complexity of these flow interactions with the underlying blowout morphology is especially visible at very short time scales (seconds or minutes), with high-frequency airflow measurements showing complex areas of airflow steering and reversing within the blowout [6,30]. Despite these significant advances in the measurement of airflow dynamics, only Smyth et al. [30] have studied sand transport within blowouts and its relationship with changes in wind characteristics and topography.

This paper studied wind and aeolian transport measurements during a 24 h, medium- to high-velocity wind event within a trough blowout located on the foredune. The purpose of this article was to understand the relationship between airflow dynamics and patterns of sediment transport from the upper beach to the established dunes under medium to high wind conditions.

2. Study Site

2.1. General Characterization

The blowout was located in the Cala Tirant coastal dune system, in the northern coast of Menorca (40°02'39" N 4°06'20" E, Balearic Islands, Spain) (Figure 1). The area is subject to a semi-arid climate, with a mean annual precipitation of 630 mm. The tidal regime is microtidal with a spring range of <0.25 m. The wave period ranges from 3 to 7 s, and waves exceeding 1 m occur for approximately 30% of the time. Occasional waves reaching up to 5 m in height are observed only during high-energy winter storm events [32] (based on data from buoy SIMAR-44 covering the period 1960–2001).

The foredune covers a surface of about 0.02 km², whilst the dune complex covers a surface of 1.6 km² approximately [33] and is limited by a marsh on its southwestern site. In this site, dunes are highly dynamic due to the strong northerlies prevailing winds called Tramuntana, with associated wind events exceeding 3.5 ms⁻¹ many days throughout the year [33]. Although winds from the north are the most significant, winds from the NNE and NNW strongly affect dune morphologies at Cala Tirant due to the morphology of the coast, which is able to modify the wind incidence in the dune system (Figure 1). The foredune reaches a maximum height of 5 m and is characterized by the presence of herbaceous vegetation, such as *Ammophila arenaria* (Figure 2). The beach is approximately 350 m long and 20 to 40 m wide.

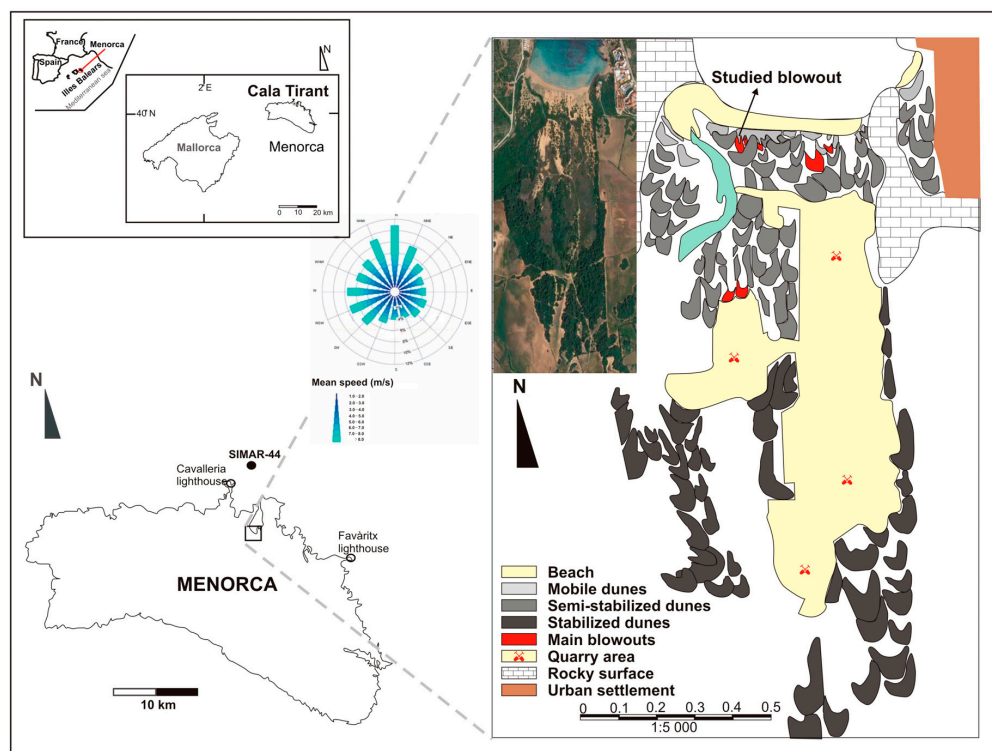


Figure 1. Location of the study site, wind direction rose, and geomorphologic sketch map of the Cala Tirant coastal dune system (Menorca, Spain).



Figure 2. Panoramic view of the embryo dunes along the first line of the dune system and the blowout.

Over many decades, the Cala Tirant beach dune system has been subject to significant human pressure and sand over-extraction. Dune erosion is mostly related to human activities such as property development, recreational activities, and poor management [20], which artificially increased the presence of blowouts along the foredune and dune system. Recent management has, however, led to a positive restoration, resulting in the formation of embryo dunes and the increase of vegetation cover [20,34]. Currently, mobile and semi-stabilized dunes cover an area of 0.13 km², with parabolic and superimposed shapes extending up to 450 m inland from the coastline [33]. Stabilized dunes were highly affected by sand quarries in the past and currently cover an area of only of 2.18 km², representing 50% of their original surface.

2.2. Blowout Characterization

The experiment was conducted within a trough blowout located within the foredune at Cala Tirant (Figure 3). The deflation basin was approximately 5.5 m, with deep respect to the erosional walls. The blowout width ranged from a minimum of 10.6 m in the northern margin to a maximum of 15.5 m at the center. The axial length was 60 m from the throat

of the foredune to the depositional lobe, with an orientation NNW-SSE (355°). The 1.5 m embryo dune in front of the blowout was slightly degraded but partially recovered over the last few years due to the growth of *Ammophila arenaria* (Figure 2). The inner part of the blowout (deflation basin and lateral walls) and the depositional lobe were free of vegetation (Figure 4C).

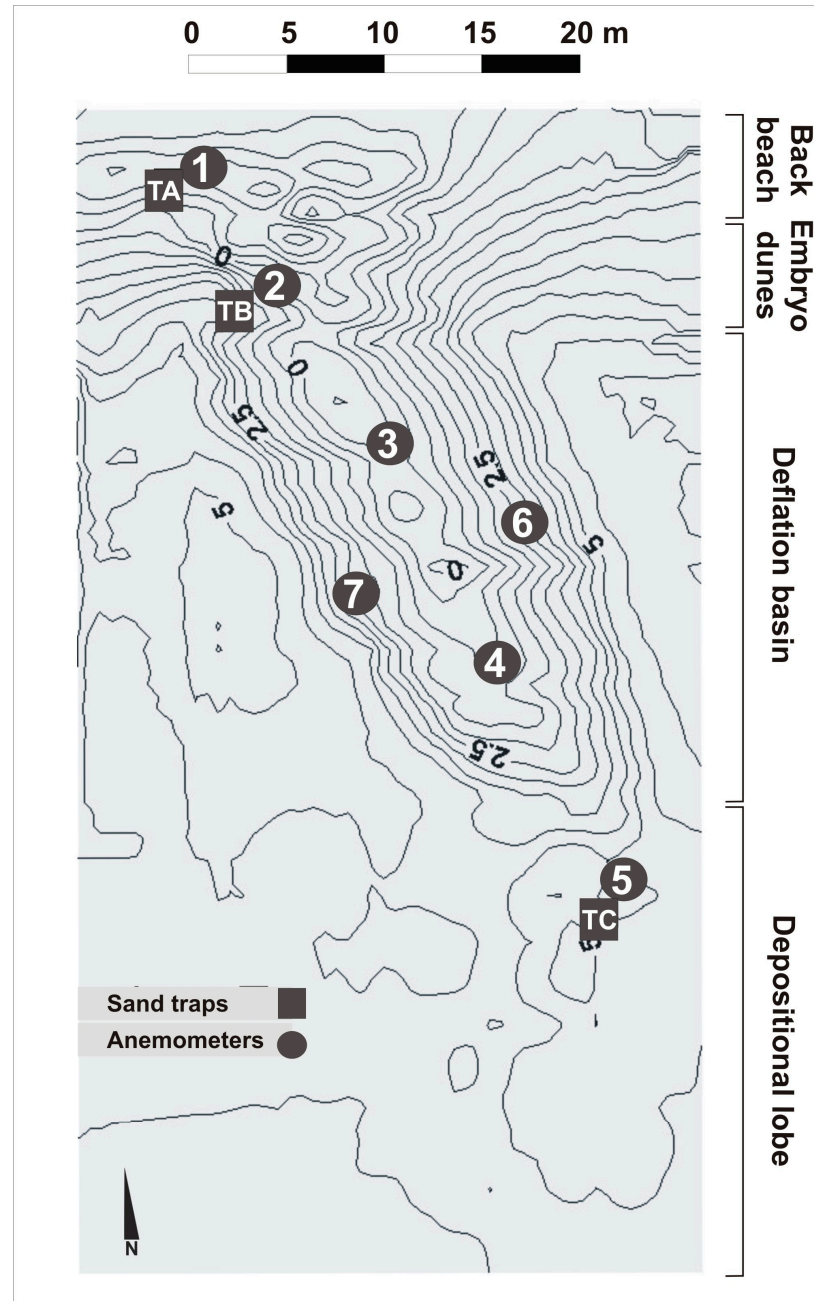


Figure 3. Plan view and topographical sketch of the beach, embryo dunes, and blowout. The locations of the anemometers and sand traps are annotated.

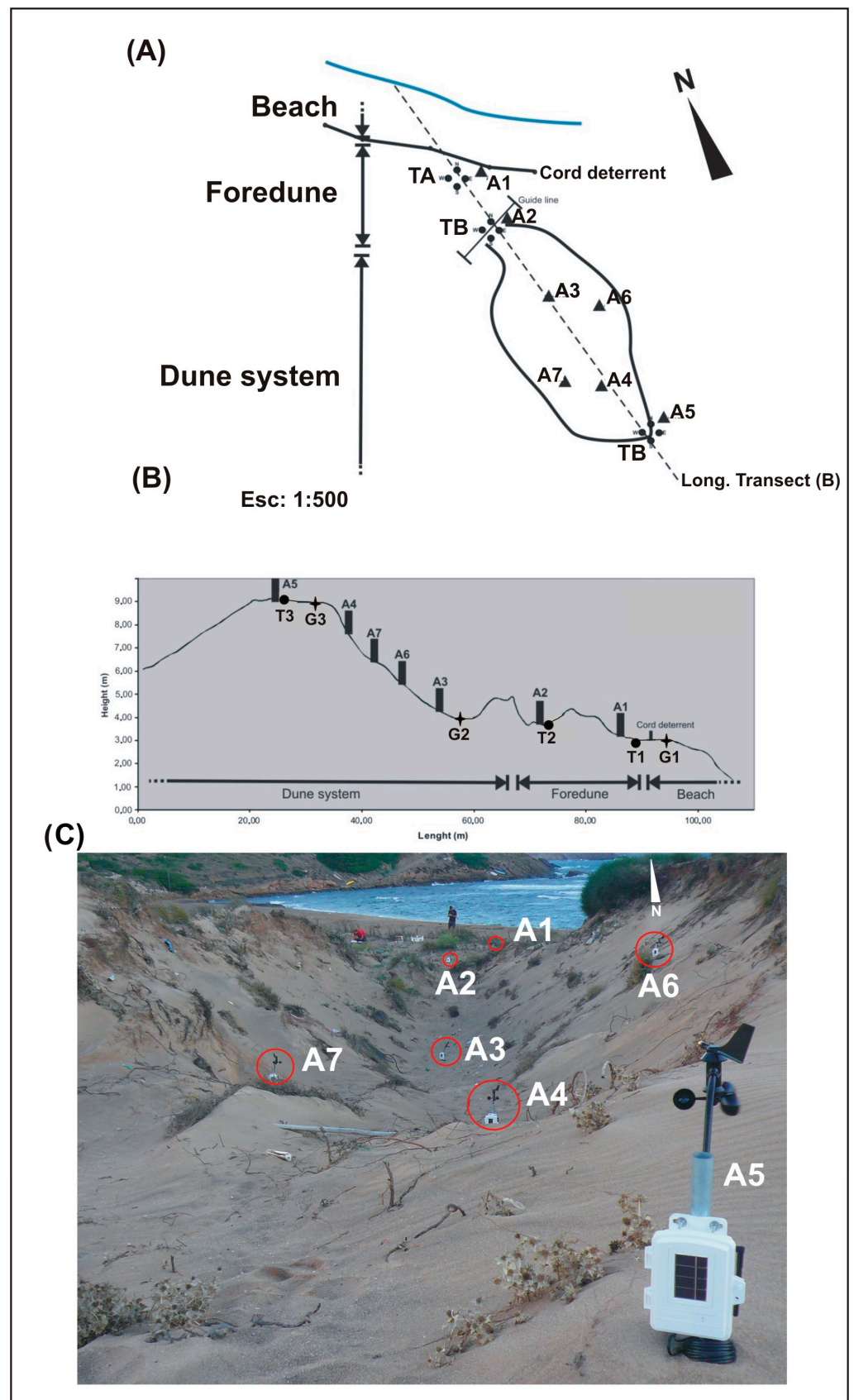


Figure 4. General view of the experiment setup: (A,B) Schematic plan and profile view of the beach and the blowout. The locations of anemometers, sand traps, and sampling points of sediment are annotated. (C) Detailed picture of the anemometers deployed on the field.

Sediment consists of medium- to coarse-grain calcareous sand. Sediment samples collected in G1, G2, and G3 (Figure 4B) showed small differences in sediment characteristics within the blowout, with mean sizes of 380.5 μ , 472.5 μ , and 484.4 μ , respectively, after [35].

3. Materials and Methods

3.1. Experiment Setup

The experiment was conducted under high-energy winter winds (maximum wind speed was 17.9 ms^{-1}) over a period of 24 h. Wind characteristics and sediment transport were measured within the deflation basin, erosional walls, and depositional lobe of the blowout. A 3D digital elevation model (DEM) was produced from topographic data collected every 0.5 m along 46 transects spaced 1.5 m apart using a Leica DGPS. Points were taken at 0.75 m of resolution along the embryo dune, blowout, and depositional lobe.

3.2. Wind Measurements

Wind data were recorded using seven 2D Davis anemometers. Each anemometer consisted of three cup speed sensors and one direction vane. Anemometers were deployed in the outer margin, within, and in the innermost part of blowout (Figure 4A,C). Mean and maximum wind speeds, mean wind direction, and air temperature were recorded at a 1 min frequency. Anemometers were deployed 0.4 m above the surface facing toward the geographical north (Figure 4). The anemometers were wireless and transmitted information directly into a main data logger Davis Envoy8x 1.0. Data processing of wind speed and direction was carried out using the Data Transfer Utility™ software package from Davis. Directions were plotted using Open Rose 0.01™ software.

Wind speeds were grouped into 13 20 min runs (Table 1), coinciding with sediment transport measurement sampling times (Section 3.3), and were normalized by incident wind speed recorded at the back beach by A1 (Figure 4A). The speed-up ratio was calculated for wind runs during the morning, afternoon, and night. The fractional speed ratio (δ_s) was calculated after Jackson and Hunt [36] and Hugenholz and Wolfe [27]:

$$\delta_s = [u_z - U_z]/U_z \quad (1)$$

where u_z is wind speed at height z , and U_z is wind speed at height z on the reference anemometer (A1) located at the beach–dune boundary. The speed-up ratio provides a metric for assessing the changes in wind speed relative to airflow entering the blowout.

3.3. Computational Fluid Dynamics Model (CFD)

The simulation and modeling of the wind flow within the blowout were executed with the open-source CFD modeling software OpenFOAM 2.2.0. following the methodology applied by Smyth et al. [6]. The modeling conducted done using two equations Re-normalized Group (RNG) κ -Epsilon turbulence model. The RNG k - ϵ model is based on Reynolds-Averaged Navier–Stokes (RANS) equations, whereby the motion of fluid is averaged over time. Simulations were run in a parallel computing cluster using forty 2.6 GHz processors and 256 GB of RAM. The computational domain was given a uniform wall roughness height (K_s) of 0.25 m and a roughness constant (C_s) of 0.4 m. The digital elevation model (DEM) used to run the wind model was the one described in Section 3.1.

3.4. Sand Transport Measurement

Sediment transport was quantified using a total of twelve vertical traps (Figure 4C) following the design by Leatherman [37]. These traps were simple to build and deploy and have been successfully used in previous studies [38–42].

Table 1. The wind speed (u_z) of each anemometer and its respective values of the fractional speed-up ratio (δs) along the 13 runs calculated. Additionally, the mean ($\delta s \chi$) and the standard deviation ($\delta s \sigma$) of the fractional speed-up ratio by each sensor and run are provided.

	Lenght	RUN_1 (09:14–09:34)		RUN_2 (10:13–10:33)		RUN_3 (11:12–11:32)		RUN_4 (12:28–12:48)		RUN_5 (14:20–14:40)		RUN_6 (15:16–15:36)		RUN_7 (16:19–16:39)		RUN_8 (17:23–17:43)		RUN_9 (18:25–18:45)		RUN_10 (20:27–20:47)		RUN_11 (22:25–22:45)		RUN_12 (00:26–00:46)		RUN_13 (03:26–03:46)		$\delta s \chi$	$\delta s \sigma$		
		u_z	Ratio (δ)	u_z	Ratio (δ)	u_z	Ratio (δ)	u_z	Ratio (δ)	u_z	Ratio (δ)																				
Anem. 1	83	8.8	0.00	8.7	0.00	10.4	0.00	10.7	0.00	10.0	0.00	8.6	0.00	6.9	0.00	5.9	0.00	3.8	0.00	2.7	0.02	1.8	0.00	2.5	0.00	2.5	0.00	2.5	0.00	0.00	0.00
Anem. 2	73	7.2	-0.18	7.1	-0.18	8.8	-0.15	9.0	-0.16	8.3	-0.17	7.2	-0.16	5.7	-0.17	4.7	-0.20	3.1	-0.18	2.2	-0.19	1.4	-0.22	2.0	-0.20	2.0	-0.20	2.0	-0.20	-0.18	0.02
Anem. 3	55	8.8	0.00	8.7	0.00	10.9	0.05	11.4	0.07	10.3	0.03	8.8	0.02	7.0	0.01	5.8	-0.02	3.8	0.00	2.6	-0.04	1.6	-0.11	2.2	-0.12	2.2	-0.12	2.2	-0.12	-0.02	0.06
Anem. 4	38	9.8	0.11	9.9	0.14	11.3	0.09	11.5	0.07	10.9	0.09	9.1	0.06	7.2	0.04	6.1	0.03	3.7	-0.03	2.7	0.00	1.6	-0.11	2.6	0.04	2.6	0.04	2.6	0.04	0.04	0.06
Anem. 5	24	6.7	-0.24	6.6	-0.24	8.4	-0.19	8.9	-0.17	7.3	-0.27	6.7	-0.22	5.8	-0.16	4.8	-0.19	4.2	0.11	2.7	0.00	2.1	0.17	1.8	-0.28	1.8	-0.28	1.8	-0.28	-0.15	0.15
Anem. 6	47	10.0	0.14	10.1	0.16	11.3	0.09	11.5	0.07	10.8	0.08	9.1	0.06	7.2	0.04	6.0	0.02	3.2	-0.16	2.2	-0.19	1.0	-0.44	2.3	-0.08	2.3	-0.08	2.3	-0.08	-0.02	0.17
Anem. 7	42	9.5	0.08	9.7	0.11	12.1	0.16	11.2	0.05	12.0	0.20	8.9	0.03	8.1	0.17	5.9	0.00	4.4	0.16	3.2	0.19	2.1	0.17	3.0	0.20	3.0	0.20	3.0	0.20	0.13	0.07
$\delta s \chi$			-0.06		0.00		0.01		-0.01		-0.01		-0.03		-0.01		-0.05		-0.02		-0.03		-0.08		-0.06		-0.06				
$\delta s \sigma$			0.15		0.16		0.13		0.11		0.16		0.11		0.12		0.10		0.13		0.13		0.22		0.16		0.16				
Anem. 1 (ref)		8.8		8.7		10.4		10.7		10.0		8.6		6.9		5.9		3.8		2.7		1.8		2.5		2.5		2.5			

Following a modification by Cabrera and Alonso [42], the traps consisted of half-buried PVC tubes, with two longitudinal openings in the sub-aerial part. One of these openings was covered with a 60 µm screen that retained moving grains. Sediment fell into a plastic bag fitted inside the trap and was located in the buried part of the trap. The trap opening had a height of 28.5 cm and a diameter of 4 cm. The traps were divided into three groups of four traps each, facing towards the north, south, east and west to maximize the sand trap from most directions. The first group (TA) was located at the back beach, the second (TB) on the outer margin of the blowout and behind the embryo dunes, and the third (TC) at the beginning of the depositional lobe (Figure 4A,B).

Sediment transport was sampled over 13 runs of 20 min each (Table 2). Following the index used by Cabrera and Alonso [42], transport rates were calculated as follows:

$$Q_{\text{trap}} = [St/d * Ts]/1000 \tag{2}$$

where St is the sediment trapped (g), d is the diameter of the sand trap (expressed in mm), and Ts is the sampling time. Transport rates in this article are expressed in kg m⁻¹ min⁻¹.

Table 2. The relationship of averages between wind velocities and sand transport amounts by each run and group of sand traps. The table was created using data from A1 as a reference for TA, A2 as a reference for TB, and A5 as a reference for TC. Wind speed is expressed in ms⁻¹ and sand transport in kg m⁻¹ min⁻¹. The orientation of the traps for each of the RUNS present the following order in the table: N, S, E, W.

	Time	Back Beach		Embryo Dunes		Depositional Lobe	
		A1	TA	A2	TB	A5	TC
		Speed	Transport	Speed	Transport	Speed	Transport
Run 1	9:14	8.3	13.89	6.9	2.915	8.3	112.925
	9:15	8.5	0.04	7.3	0.06	8.6	0.225
	9:16	9.4	1.825	7.7	0.395	9.2	1.575
	9:17	9.1	4.785	7.7	0.575	9.6	50.91
Run 2	10:13	8.5	23.015	7	2.28	8.4	111.835
	10:14	7.7	0.17	6.9	0.015	8.1	0.58
	10:15	8.9	0.92	7.2	0.415	9.2	0.67
	10:16	8.3	0.41	6.5	0.97	7.8	57.465
Run 3	11:12	9.7	57.655	7.8	22.79	9.8	113
	11:13	9.1	4.395	7.7	1.695	9.3	6.3
	11:14	10.2	2.625	8.3	4.26	10.7	2.245
	11:15	11.1	1.79	9.4	15.76	12.3	64.285
Run 4	12:28	9.7	58.29	7.9	30.31	10.4	100.18
	12:29	10.3	1.79	8.6	12.195	10.7	3
	12:30	10.6	1.195	8.8	2.135	11.6	0.855
	12:31	10.6	1.57	9.4	19.455	11.8	64.625
Run 5	14:20	10.4	21.93	9	6.1	10.8	100.665
	14:21	10.5	2.575	8.5	4.225	10.8	7.37
	14:22	10.4	0.655	9	0.725	11.1	8.135
	14:23	9.9	0.445	8.5	2.68	10.5	71.64
Run 6	15:16	8.9	2.125	7.8	0.385	9.5	56.75
	15:17	9.5	0.425	7.7	2.82	9.8	10.605
	15:18	9.7	0.235	8	0.075	10.1	2.64
	15:19	8.8	0.055	8	0.22	9.6	42.83

Table 2. Cont.

	Time	Back Beach		Embryo Dunes		Depositional Lobe	
		A1	TA	A2	TB	A5	TC
		Speed	Transport	Speed	Transport	Speed	Transport
Run 7	16:19	7.9	0.05	6.4	0.035	7.4	18.99
	16:20	7.2	0.56	6.2	0.5	7.8	1.175
	16:21	8	0.005	6.5	0.03	8	0.125
	16:22	7.4	0.01	6.6	0.05	7.7	2.15
Run 8	17:23	7	0.045	5.9	0	6.6	11.745
	17:24	6	0.110	5.1	0.145	6.1	0.03
	17:25	6.7	0.030	5.6	0	6.4	0.085
	17:26	7	0.030	5.5	0.065	6.5	0.13
Run 9	18:25	4.5	0.030	3.7	0.065	4.5	9.785
	18:26	4.1	0.075	3.4	0.085	4.1	0.02
	18:27	4.1	0.015	3.2	0	4.1	0.065
	18:28	4.4	0.020	3.8	0.04	4.7	0.105
Run 10	20:27	1.5	0.020	1.5	0.03	1.4	7.095
	20:28	1.6	0.055	1.6	0.07	1.8	0.015
	20:29	2.4	0.015	1.7	0	2.1	0.045
	20:30	2.4	0.015	1.7	0.03	2.3	0.075
Run 11	22:25	1.9	0.010	1.4	0.005	1.6	2.050
	22:26	2	0.005	1.7	0.01	1.8	0.010
	22:27	2	0.005	1.5	0	1.9	0.030
	22:28	1.8	0.005	1.6	0.015	1.8	0.050
Run 12	0:26	4.3	0.025	3.5	0.06	3.9	5.87
	0:27	3.7	0.005	3.1	0.045	3.7	0.01
	0:28	4.2	0.010	3.3	0	3.7	0.035
	0:29	3.9	0.015	3.1	0.035	4	0.06
Run 13	3:26	3.1	0.010	2.5	0.005	3	1
	3:27	2.8	0.005	2.2	0.01	2.7	0.005
	3:28	2.2	0.005	1.6	0	2.1	0.025
	3:29	2.4	0.005	1.8	0.02	2.1	0.04

4. Results

4.1. Wind Characterization

4.1.1. Mean and Maximum Wind Speed

Spatially, winds were strongest (both mean and maximum speeds) in the distal slope right before the depositional lobe (anem. 4) and lateral walls (anem. 7 and 6). Wind speeds were lowest in the lee of the embryo dune (anem. 2) and depositional lobe (anem. 5).

Temporally, maximum wind speeds up to 17.9 ms⁻¹ were recorded at approximately 12:02 p.m. by anem. 4. Wind speeds decreased from 02:00 p.m. and reached a minimum (close to 0 ms⁻¹) between 04:30 and 08:56 a.m. The relative behavior of wind speeds recorded by different anemometers over time was globally similar (Figure 5), with a generalized decrease of wind speed from 02:00 p.m.

4.1.2. Wind Direction

Wind direction recorded by each anemometer (Figures 6 and 7) was relatively constant both in time and space, oscillating between 250° and 350° (WSW-NNW) throughout most of the experiment. Wind direction switched to 50–200° (NE-SSW) at 05:00 a.m. at all locations, except for A7, coinciding with the decrease of air temperature and wind speed described in Section 4.1.1.

Despite relatively constant wind directions, topographic wind steering was visible within the blowout. Figure 7 summarizes wind direction over the 24 h sampling period

and shows a relatively constant onshore incoming wind direction from the NW at the back beach (A1), roughly aligned with the blowout's throat. Flow was steered towards NNW at A2, where the presence of vegetation (*Ammophila arenaria*) at the embryo dune generated secondary directions from N and NE. Winds were from the NW again at A3 and A4 due to incident wind direction and significant canalization of the flow following Bernoulli's principle or the Venturi effect. Wind direction was relatively constant from the NW at A5, with secondary directions from NNW and WNW. The largest changes in wind direction occurred at A6 (E wall) (Figure 7B), with W to SW winds almost perpendicular to the wall orientation (N-S). Wind direction was constant at A7 (W wall) (Figure 7B) and remained steady and constantly steered from the N-NW at that location, despite drastic changes in incoming wind directions during the last hours of the experiment (Figure 6).

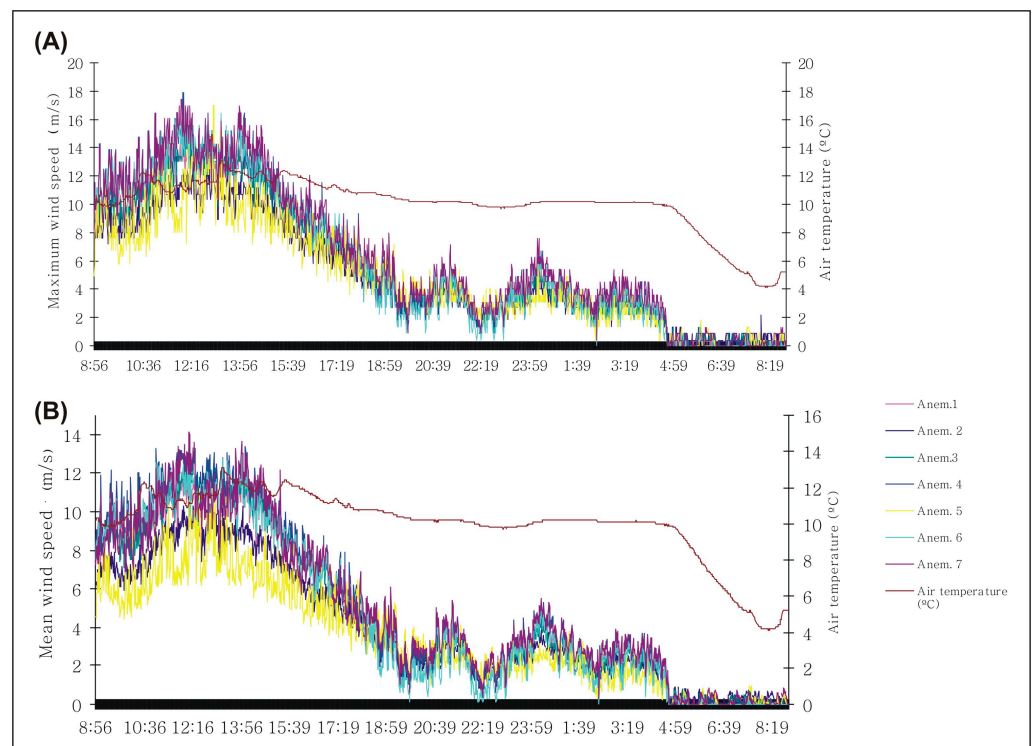


Figure 5. Wind speed distribution over 24 h of sampling: (A) 1 min averages of maximum wind speed throughout the experiment period; (B) 1 min averages of mean wind speed throughout the experiment period (values expressed in ms^{-1}).

4.1.3. Fractional Speed-Up Ratio

Figure 8 shows the spatial distribution of fractional speed-up ratios (δs) during the morning (runs 1–5), afternoon (runs 6–10), and night (runs 11–13). Winds were slower in comparison with incoming wind speeds at the embryo dune (A2; average $\delta s_{\chi} = -0.15$) and depositional lobe (A5; average $\delta s_{\chi} = -0.2$) for all runs (Table 1). The magnitude of wind speed in the blowout basin was generally closer to incoming wind speeds, but there were considerable oscillations depending on the moment of the day. At A3, winds were accelerated in the morning with respect to winds measured in location A1 ($\delta s = 0.07$), similar to incoming wind speeds in the afternoon ($\delta s = 0.00$), but significantly slower during the night ($\delta s = -0.15$). Winds at A4 (upper slope of the deflation basin just before the depositional lobe) were the strongest throughout the majority of the experiment, with the exception of runs 9–11. Wind speed behavior during these three runs was considerably different from the rest of the experiment, with wind speeds now being the strongest at the depositional lobe (A5) and significantly lower at the upper slope of the deflation basin (A4).

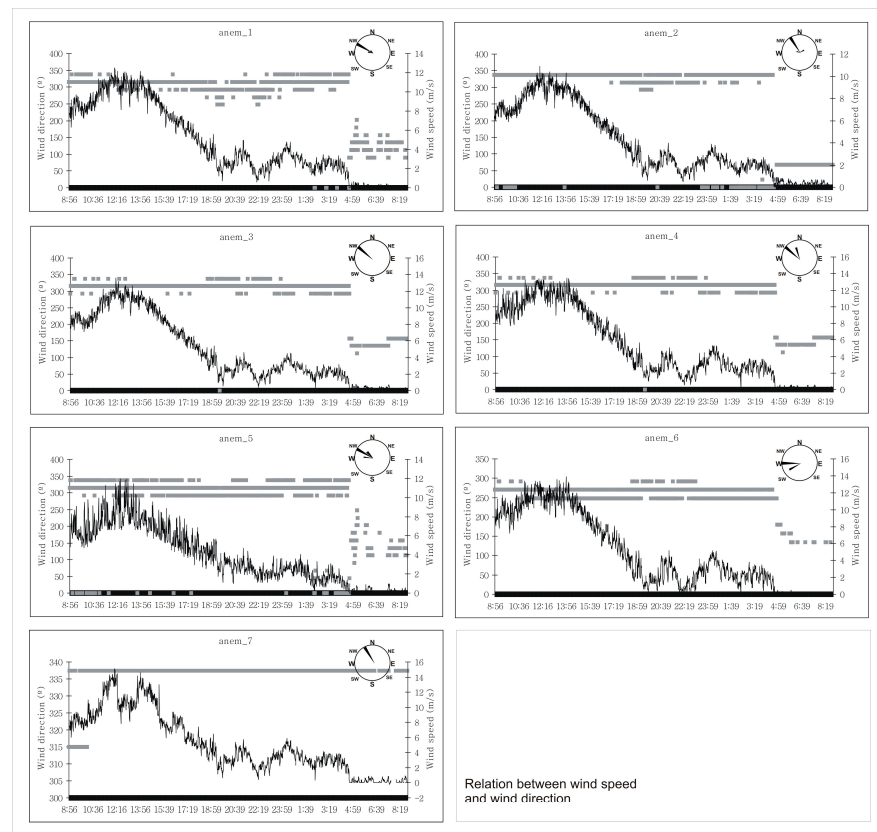


Figure 6. Relationship between wind speed and direction registered by each anemometer throughout the 24 h of experiment. Gray blocks and the wind roses represent wind directions.

4.1.4. Patterns of Sediment Transport

Figure 9 shows temporal changes of aeolian sediment transport as measured by the traps during the morning, afternoon, and night. Transport was largest during the morning (runs 1 to 5), coinciding with the strongest winds (Figure 5). It gradually decreased during the afternoon (runs 6–10), as the wind speed decreased, and it was lowest at night (runs 11–13) when the winds slowed down (Table 2). The largest transport rates were registered by TC5 ($Q = 46.95 \text{ kg m}^{-1} \text{ min}^{-1}$) and the smallest by TA11, TB11, and TA12 (approximately $Q = 0.01 \text{ kg m}^{-1} \text{ min}^{-1}$ (Table 3)).

Table 3. Amounts of sediments captured by each group of sand traps deployed along the thirteen runs carried out on the experiment.

Run	TA	TB		TC
		Values in $\text{kg m}^{-1} \text{ min}^{-1}$		
1	5.14	0.99		41.41
2	6.13	0.92		42.64
3	16.62	11.13		46.46
4	15.71	16.02		42.17
5	6.40	3.43		46.95
6	0.71	0.88		28.21
7	0.16	0.15		5.61
8	0.05	0.07		3.00
9	0.04	0.05		2.49
10	0.03	0.03		1.81
11	0.01	0.01		0.54
12	0.01	0.035		1.494
13	0.006	0.009		0.268

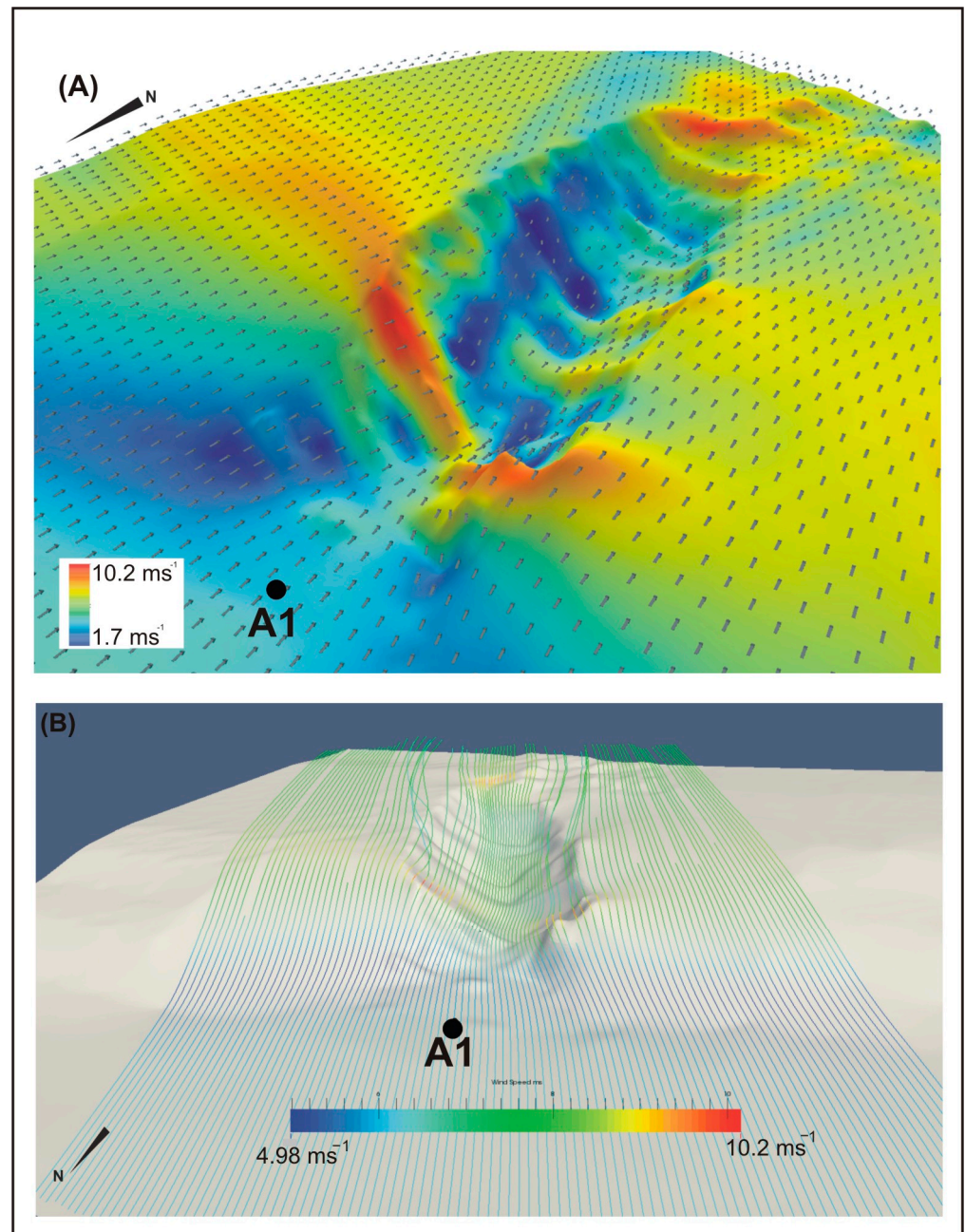


Figure 7. (A) Wind direction and speed computational fluid dynamic (CFD) model at 1 m above the surface and with 350° on anemometer 1. Arrows are in 2 m intervals, indicating flow direction at 0.4 m above the surface, while the color gradient shows its velocity. (B) Aeolian flow simulation from the wind of 350° at 1 m above surface.

Mean sediment transport rates during the morning were $TA_Q = 10 \text{ kg m}^{-1} \text{ min}^{-1}$, $TB_Q = 6.5 \text{ kg m}^{-1} \text{ min}^{-1}$, and $TC_Q = 43.9 \text{ kg m}^{-1} \text{ min}^{-1}$. Maximum transport rates were during runs 3, 4, and 5 (Table 4). Mean transport rates during the afternoon were lower than those during the morning, with $TA_Q = 0.24 \text{ kg m}^{-1} \text{ min}^{-1}$, $TB_Q = 0.28 \text{ kg m}^{-1} \text{ min}^{-1}$, and $TC_Q = 39.3 \text{ kg m}^{-1} \text{ min}^{-1}$. Sediment transport was almost non-existent at night due to mean wind speeds lower than 3 ms^{-1} , resulting in average transport rates of $TA_Q = 0.014 \text{ kg m}^{-1} \text{ min}^{-1}$, $TB_Q = 0.021 \text{ kg m}^{-1} \text{ min}^{-1}$, and $TC_Q = 1.02 \text{ kg m}^{-1} \text{ min}^{-1}$. It is worth noting that small amounts of transport were recorded with wind speeds below 2.5 ms^{-1} at TC11.

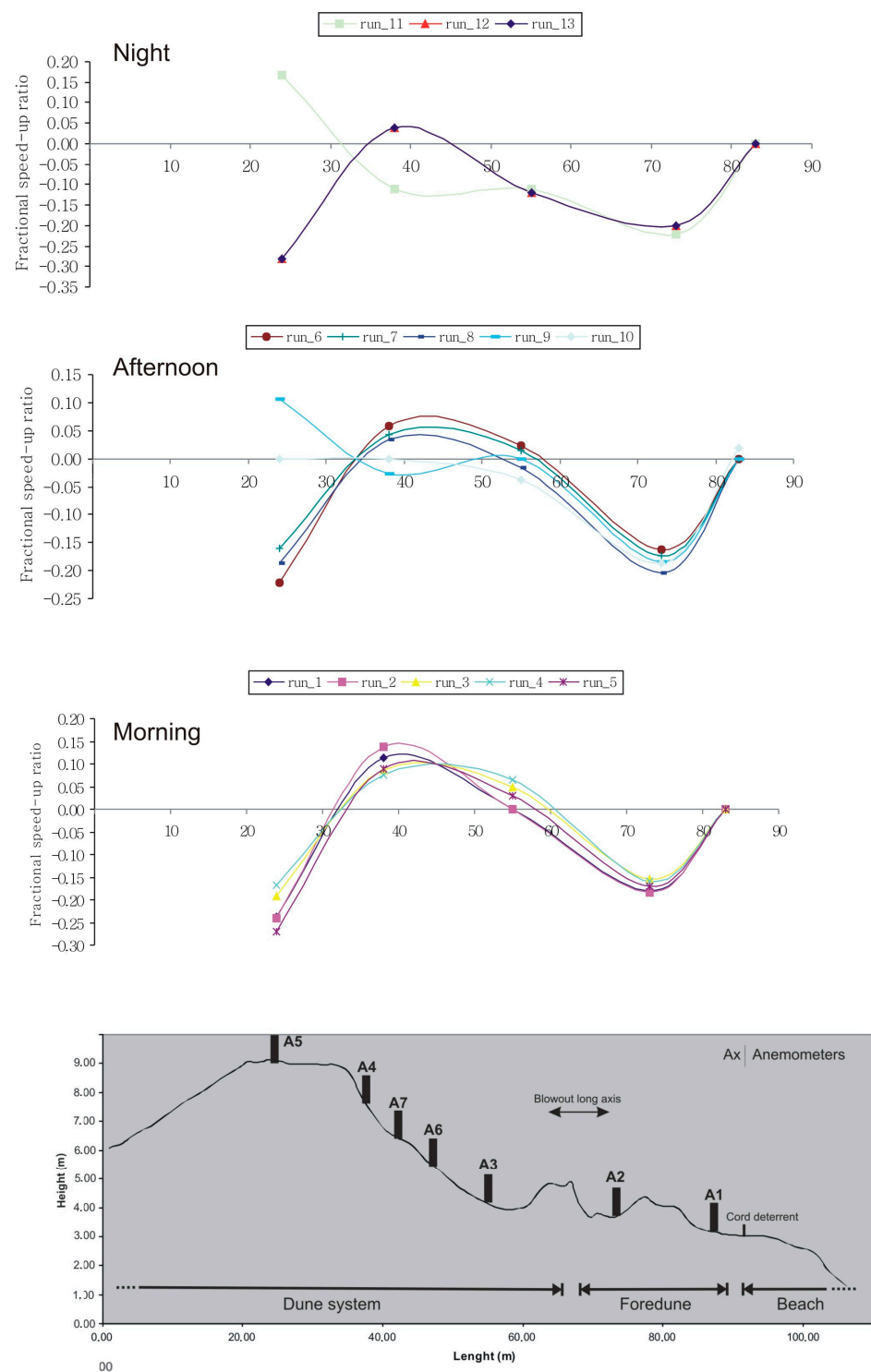


Figure 8. Time-average wind speeds (fractional speed-up ratios) in the blowout for anemometers 1, 2, 3, 4, and 5 using anemometer 1 as a reference (after Jackson and Hunt [36]; Hugenholtz and Wolfe [27]). Anemometers 6 and 7 are included in the speed-up ratio (see Table 1) but were not represented in the figure because they were not deployed in the same axis (see location in Figure 3). The results were divided into three different times (morning, afternoon, and night) according to the wind velocities along the experiment.

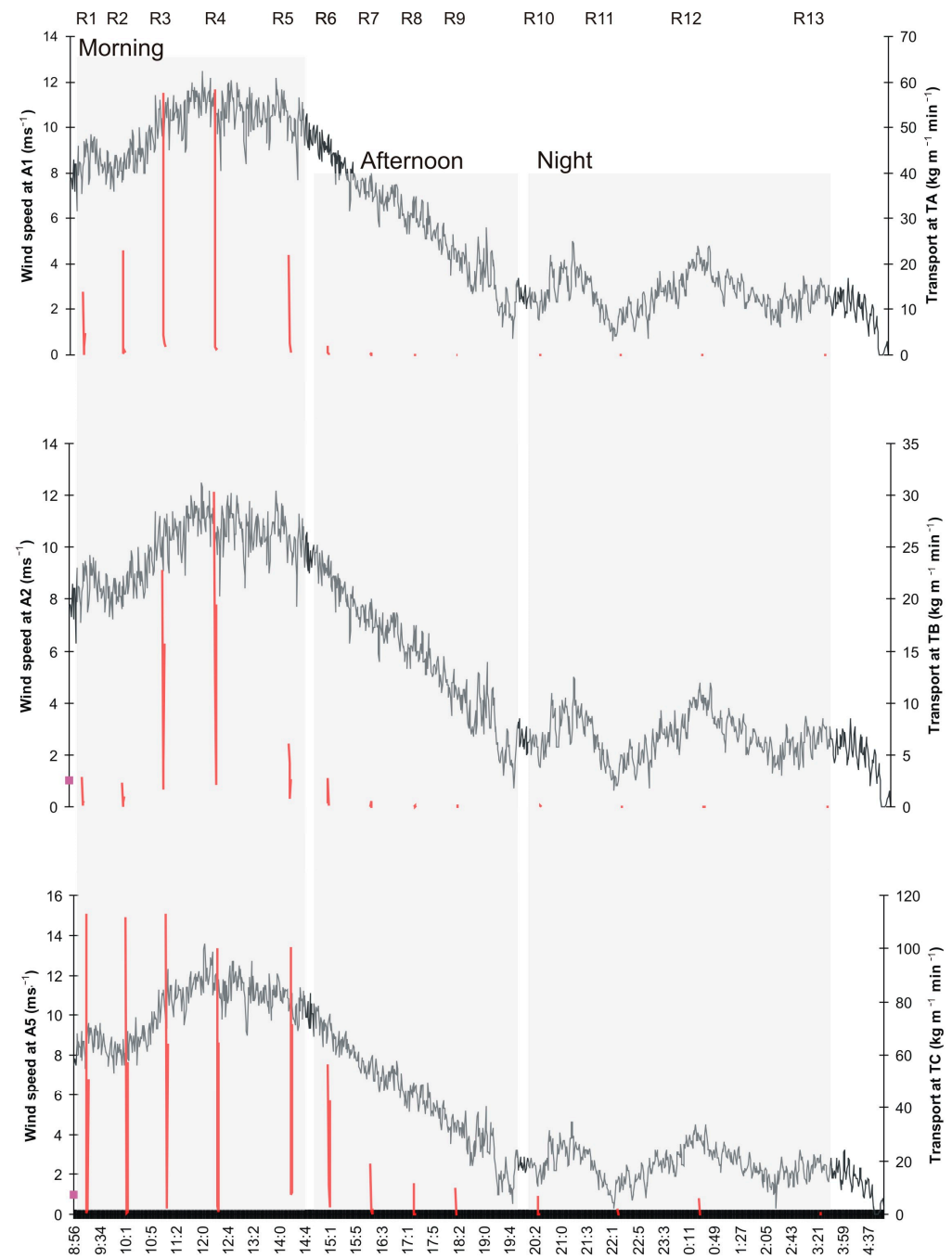


Figure 9. The relationship between wind velocities and sand transport amounts. The graphs were created using data from A1 as a reference for TA, A2 as a reference for TB, and A5 as a reference for TC. Each of the red lines correspond to one of the runs and represent the total amount of sand caught by each group of traps. The gray line represents wind speed over the entire 24 h experiment.

Figure 10 shows spatial changes in sediment transport rates for all runs. Transport rates were consistently larger at TC in the depositional lobe, not at TA where there were relatively stronger winds (Figure 8; Section 4.1.3). The lowest transport rates were measured by TB. This spatial pattern was relatively constant over time, although runs 3 and 4 experienced an increase of sand flux at TA and TB corresponding with increasing wind speeds (Figure 5).

Table 4. Sand captured by each group of traps along the different sampling times.

Time	Run	Qtrap (kg m ⁻¹ min ⁻¹)
Morning	TA1	5.14
	TB1	0.99
	TC1	41.41
	TA2	6.13
	TB2	0.92
	TC2	42.64
	TA3	16.62
	TB3	11.13
	TC3	46.46
	TA4	15.71
	TB4	16.02
	TC4	42.17
	TA5	6.40
	TB5	3.43
	TC5	46.95
Afternoon	TA6	0.71
	TB6	0.88
	TC6	28.21
	TA7	0.16
	TB7	0.15
	TC7	5.61
	TA8	0.05
	TB8	0.07
	TC8	3.00
TA9	0.04	
TB9	0.05	
TC9	2.49	
Night	TA10	0.03
	TB10	0.03
	TC10	1.81
	TA11	0.01
	TB11	0.01
	TC11	0.54
	TA12	0.01
	TB12	0.035
	TC12	1.494
TA13	0.006	
TB13	0.009	
TC13	0.268	

Figure 10B summarizes the spatial-temporal patterns of sediment transport during the experiment. There were significant differences between TC and TA-TB, especially during the morning. Transport rates peaked during runs 3, 4, and 5, with values at TC over 45 kg m⁻¹ min⁻¹. Transport decreased during runs 6 (TC = 28.21 kg m⁻¹ min⁻¹) and 7 (TC = 5.61 kg m⁻¹ min⁻¹) (Table 4), coinciding with decreasing wind speeds (Figure 5). The total sand collected by traps over 24 h was TA = 51 kg, TB = 33.71 kg, and TC = 263 kg.

Strong winds from 09:00 a.m. to 02:00 p.m., almost perpendicular to the E wall (A6, Figure 7), were associated with recurrent sand slides that slightly modified the inner topography of the blowout (Figure 11A). Winds were almost parallel to the W wall (A7, Figure 7), which, in this case, resulted in the strong erosion and transport of material away from the wall, preventing sand avalanching (Figure 11B).

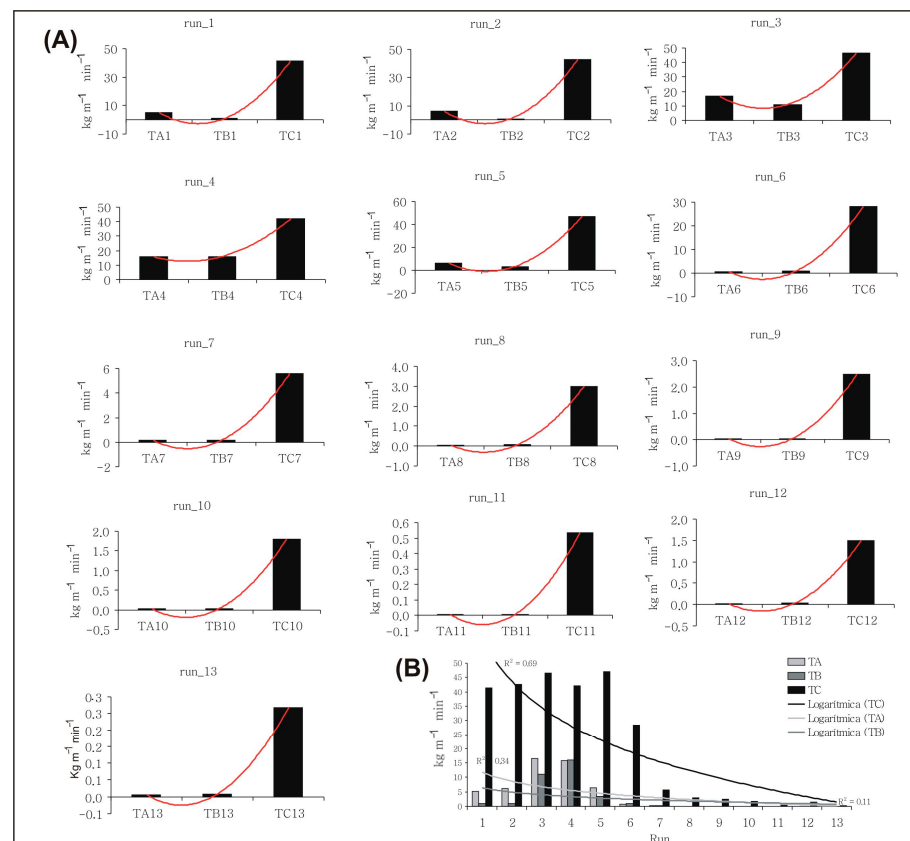


Figure 10. Spatial patterns of sediment transport captured by TA, TB, and TC: (A) sediment transport occurred in each of the 20 min runs carried out; (B) overview of the spatial differences of sediment captured over the 24 h of the experiment.

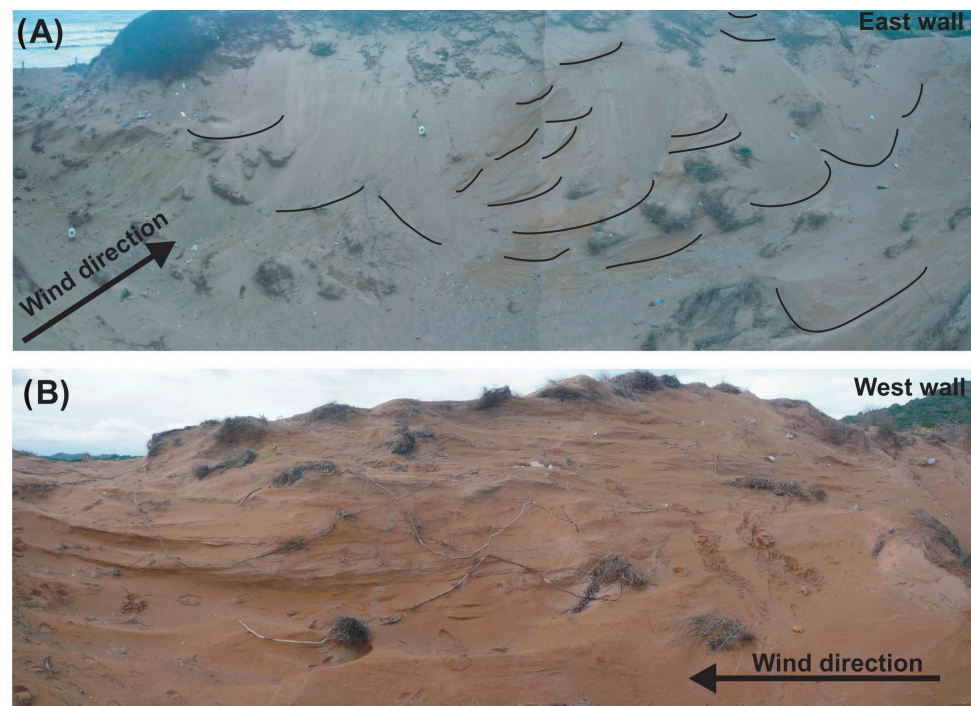


Figure 11. General views of the lateral walls within the blowout: (A) east wall, with a perpendicular wind incidence, which caused significant detachments; (B) west wall, with a parallel wind direction, causing a significant undermining of sediment.

5. Discussion

5.1. Wind Flow and Topographic Control

In line with previous studies [6,30,31], this research showed that topography exerts an important control on airflow within blowouts. Winds were stronger at the blowout throat and deflation basin due to airflow compression following Bernoulli's principle (Figure 8). This was followed by flow expansion and divergence at the depositional lobe and a decrease in wind speed. Different patterns of wind steering within the blowout can lead to different modes of sediment transport. During the same event, perpendicular winds at the E wall generated relatively constant sand slides, while parallel winds along the W wall eroded the sediment and transported it away towards the depositional lobe (Figure 11).

As found by other authors [2,29,30,39], there were significant spatial differences in wind speeds within the blowout. The strongest winds were measured at the upper slope of the deflation basin (A7 and A4) as a result of channeled airflows (see location on Figure 4A).

Several studies have noted that airflow behavior is dependent upon blowout form. In trough blowouts [2,43], the wind accelerates within the blowout throat, whilst, in saucer and bowl blowouts, a separation zone develops in the lee of the blowout crest, increasing the airflow complexity [27,31]. In bowl blowouts, unlike in trough blowouts, the flow expands and decelerates along the deflation basin [27,44]. The results obtained in this study confirm the strong control that the topography exerts on airflow within a trough blowout, whereby the presence of steep erosional walls induce wind speed-up and relatively constant wind directions along the deflation basin because of the static pressure exerted by the lateral walls of the blowout.

Fractional speed-up ratios [27,36] showed a gradual increase in wind speed with distance along the deflation basin to a maximum value just before the depositional lobe at A4 (Section 4.1.3). This increase in wind speed along the deflation basin has been previously observed in a diversity of blowout environments [6,27,31]. It is worth noting, in this study, that incoming onshore wind speeds were consistently stronger at the back beach (A1) than in the lee of the embryo dune located at the opening of the blowout (A2; Figure 8). While the lower wind speeds at this location demonstrate the effect of the embryo dune topography on incoming airflow, wind direction was only partially steered at this location, suggesting that embryo dune morphology and height were not enough to induce airflow separation and reversal.

5.2. Transport and Supply Limiting Factors

The results obtained from this study show good correspondence between temporal variations in wind speed and sand transport rates within the blowout. However, spatial variations in wind speed did not correspond well with measured sand transport rates. The largest sediment transport rates were recorded at the upper margin of the blowout (TC), on the depositional lobe, where the wind was slowest (A5, Figure 8). TC and A5 were located in a region of flow expansion and wind speed reduction. Although transport was not quantified at A3 and A4, visual observations, as Figure 11 shows, permitted the identification of large amounts of sediment erosion from the deflation basin during strong winds. Thus, sediment that had been entrained along the deflation basin of the blowout was being deposited at this location on the depositional lobe. Additionally, and in line with Hesp and Walker [31], the erosion of the lateral walls and deposition of sediment on the deflation basin helped increasing the budget of sand available for transport toward the depositional lobe.

Small sediment fluxes were measured at TA (back beach) under wind speeds that were considerably higher than TC. With no rain or moisture limiting sediment availability in this area, the main limiting factor was a short fetch distance due to a narrow beach.

Low sediment transport rates recorded at TB were due to increases of surface rugosity due to the presence of the foredune and vegetation reducing wind speeds.

However, Figure 10 shows relatively large transport rates in TA and TB during runs 3 and 4, coinciding with the strongest winds ($10\text{--}12\text{ ms}^{-1}$) measured at A1 (Figure 5).

Hence, even in the presence of limiting factors such as short fetch distances and foredune topographies and vegetation, wind speeds over 10 ms^{-1} can entrain and transport sediment from the upper beach into the dune complex.

To date, sand transport patterns within blowouts are still not well understood. Jungerius and van der Meulen [45] observed a decrease in erosive power from a maximum at the outer margin to lower values within the blowout due to development of transport. Hesp and Walker [31], however, suggested more complex transport dynamics, with secondary flow patterns resulting in multi-directional transport within the entire blowout and beyond. The results presented in this study support findings by Hesp and Walker [31] and suggest the development of complex transport patterns with avalanching and/or removal from lateral walls, erosion in the deflation basin, and large deposition despite lower winds at the depositional lobe.

5.3. Implications for Management

The presence of vegetation along the first line of coastal dunes can play an important role in the development of dune systems [46–51]. Mir-Gual et al. [7] linked the conservation state of the first line of dunes in the Balearic Islands with the presence/absence of psammophyte vegetation, where well-preserved foredunes are well-vegetated. Vegetation has an important role in aeolian sediment dynamics because it decreases the near-surface wind speed and enhances the sediment deposition. In line with other authors (e.g., [8,46,52]), our results suggest that the presence of vegetation in the outer margin of the blowout increased the sand surface rugosity, which decreased wind speed and enhanced sediment deposition (sensors A2 and TB). The presence of a relatively low, vegetated dune at the beginning of the throat did not seem to limit the movement of sediment within the blowout under medium to high wind speeds. While little transport was recorded at TB, the depositional lobe received large amounts of sediment over 24 h, and active transport was visible in the blowout walls and deflation basin. Our results suggest that management techniques that lead to the positive restoration of foredunes in Balearic Islands could perfectly co-exist with the preservation of un-vegetated, active blowouts in the dune fields. Blowouts intersecting the first line of coastal dunes may lead to an output of sand from the beach into the blowout through aeolian processes. In the context of the Balearic Islands, this output is considered 'negative' from a management perspective, as the beach is an essential touristic and economic resource. This has triggered the active restoration of embryo dunes and foredunes through an increase of vegetation cover over the last few years [20,34]. The results presented in this paper suggest that, while this restoration leads to a relative closure of the blowout from the beach (e.g., possible decrease of sediment input to the blowout), the interaction between wind, topography, and available sediment within the blowout maintains active transport patterns that result in a very dynamic blowout behavior during short-term events.

6. Conclusions

This study aimed to increase the knowledge about airflow dynamics and patterns of sediment transport from the beach to established dunes through a trough blowout. Despite low sediment transfer from the beach to the blowout due to the presence of an embryo dune, substantial amounts of sediment transport were measured from the deflation basin toward the depositional lobe.

In relation to the wind and topography relationship, two features should be taken into account. First, embryo dunes and herbaceous vegetation (e.g., *Ammophila arenaria*) in the outer margin of the blowout increased surface rugosity, which in turn decreased wind speed and induced flow complexity. Second, the blowout throat generated a channelization of the air flow along the deflation basin, which, helped by the inner morphometry of blowout and according to de Venturi's effect, increased wind speed and consequently sediment entrainment and transport. Once the airflow reached the upper margin of the blowout, it expanded and decelerated, which led to sediment deposition.

The present work demonstrated two different erosion processes, which, depending on the angle of incidence of wind flow on the lateral walls of the blowout, generated different sedimentary behaviors. On the east wall, with perpendicular winds, sediment tended to collapse in the form of small sand slides. Due to the force of gravity, sediment was gradually deposited on the deflation basin to be later transported by the flow to the innermost section. In contrast, on the western wall, parallel winds progressively dismantled the wall and directly transported sand toward the depositional lobe.

The patterns of sediment transport are highly conditioned by: (a) wind characteristics (speed and direction) and (b) by the topography of the blowout and surrounding areas. Our results demonstrated how complex the wind–sediment transport relationship is. For example, the place where the largest sediment transport rates were recorded (at the upper rim of blowout, in the depositional lobe) did not coincide with the point of highest wind speeds (deflation channel). While the deflation channel acted as an area of sediment entrainment and erosion, the depositional lobe acted as an area of sediment accumulation. Limiting factors, such as fetch distances and increases in roughness rugosity, decreased aeolian sediment transport at the back beach and behind the foredune, respectively.

Finally, in places like the Balearic Islands, sand output from the beach into coastal blowouts is considered ‘negative’ from a management perspective, as the beach is an essential touristic and economic resource. Results in this paper suggest that the restoration of the first line of dune (foredune strip) could limit the amount of sand blown from the beach but could still permit dynamic blowout and dune behavior landward of the foredune.

Although the main goal of this study was to focus on the sedimentary behavior under a medium–high energy episode, it would be interesting for future works to address this aspect over a longer time scale with the purpose of continuing to advance and improve the knowledge of the relationship between blowouts and sediment transport patterns.

Author Contributions: Conceptualization, M.M.-G., G.X.P. and I.D.-F.; Methodology, M.M.-G., G.X.P., I.D.-F. and T.A.G.S.; Software, T.A.G.S.; Validation, G.X.P., I.D.-F. and T.A.G.S.; Investigation, M.M.-G.; Resources, M.M.-G.; Data curation, M.M.-G.; Writing—original draft, M.M.-G.; Writing—review & editing, M.M.-G., G.X.P., I.D.-F. and T.A.G.S. All authors have read and agreed to the published version of the manuscript.

Funding: This study was carried out through the Chronic Emergencies and Ecosocial Transformations in Touristified Coastal Spaces (PID2022-137648OB-C21) project, funded by MCIN/AEI/10.13039/501100011033 (Spanish Ministry) and by “ERDF A way of making Europe”.

Informed Consent Statement: Not applicable.

Data Availability Statement: The data presented in this study are available upon request from the corresponding author. The data is not publicly available due to not being on any access platform.

Acknowledgments: The authors are indebted to the helpful comments of the anonymous referees whose assessments greatly improved the original manuscript.

Conflicts of Interest: The authors declare no conflict of interest.

References

1. Bagnold, R.A. *The Physics of Blown Sand and Deserts Dunes*; Methuen: London, UK, 1954; p. 265.
2. Hesp, P. Flow dynamics in trough blowout. *J. Bound. Layer Meteorol.* **1996**, *77*, 245–268. [[CrossRef](#)]
3. Bate, G.; Ferguson, M. Blowouts in coastal foredunes. *Landsc. Urban Plan.* **1996**, *34*, 215–224. [[CrossRef](#)]
4. Hesp, P.; Hyde, R. Flow dynamics and geomorphology of trough blowouts. *Sedimentology* **1996**, *43*, 505–525. [[CrossRef](#)]
5. Davis, J.R.; Fitzgerald, D.M. *Beaches and Coasts*; Blackwell Publishing: Carlton, Australia, 2004; p. 432.
6. Smyth, T.A.G.; Jackson, D.W.T.; Cooper, J.A.G. High resolution measured and modelled three-dimensional airflow over a coastal bowl blowout. *Geomorphology* **2012**, *177*, 62–63. [[CrossRef](#)]
7. Mir-Gual, M.; Pons, G.X.; Martín-Prieto, J.A.; Roig-Munar, F.X.; Rodríguez-Perea, A. Geomorphological and ecological features of blowouts in a western Mediterranean coastal dune complex: A case study of Es Comú de Muro beach-dune system on the island of Mallorca, Spain. *Geo.-Mar. Lett.* **2013**, *33*, 129–141. [[CrossRef](#)]
8. Hesp, P. Foredunes and blowouts: Initiation, geomorphology and dynamics. *Geomorphology* **2002**, *48*, 245–268. [[CrossRef](#)]

9. Glenn, M. Glossary: A Study of Global Sand Seas. In *US Geological Surveys Professional Paper*; McKee, E.D., Ed.; U.S. Government Printing Office: Washington, DC, USA, 1979; pp. 399–407.
10. Carter, R.W.; Hesp, P.; Nordstrom, K.F. Erosional Landforms and Coastal Dunes. In *Coastal Dunes: Form and Processes*; Nordstrom, K.F., Psuty, N.P., Carter, R.W., Eds.; John Wiley: London, UK, 1990; pp. 217–249.
11. Smith, H.T. Physiography and Photo Interpretation of Coastal Sand Dunes. In *Final Report NONR-2242 (00)*; Office of Naval Research, Geographical Branch: Arlington, VA, USA, 1960; p. 60.
12. Ritchie, W. The evolution of coastal sand dunes. *Scott. Geogr. Mag.* **1972**, *88*, 19–35. [[CrossRef](#)]
13. Cooper, W.S. *Coastal Sand Dunes of Oregon and Washington*; Geological Society of America: Boulder, CO, USA, 1958; p. 169.
14. Bird, E. *Coastal Geomorphology. An Introduction*; John Wiley & Sons: London, UK, 2008; p. 411.
15. Gutiérrez-Elorza, M.; Desir, G.; Gutiérrez-Santolalla, F.; Marín, C. Origin and evolution of playas and blowouts in the semiarid zone of Tierra de Pinares (Duero Basin, Spain). *Geomorphology* **2005**, *72*, 177–192. [[CrossRef](#)]
16. Esler, A.E. Manawatu sand dune vegetation. *Proc. N. Z. Ecol. Soc.* **1970**, *17*, 41–46.
17. Patriquin, D.G. “Migration” of blowouts in seagrass beds at Barbados and Carriacou, West Indies, and its ecological and geological implications. *Aquat. Bot.* **1975**, *1*, 163–189. [[CrossRef](#)]
18. Harris, C. Wind speed and sand movement in a coastal dune environment. *Area* **1974**, *6*, 243–249.
19. Jennings, J.N. On the orientation of parabolic U-dune. *Geogr. J.* **1957**, *124*, 474–480. [[CrossRef](#)]
20. Roig-Munar, F.X.; Rodríguez-Perea, A.; Martín-Prieto, J.A.; Pons, G.X. Soft management of beach-dune systems as a tool for their sustainability. *J. Coast. Res.* **2009**, *SI56*, 1284–1288.
21. van Boxel, J.H.; Jungerius, P.D.; Kieffer, N.; Hample, N. Ecological effects of reactivation of artificially stabilized dunes. *J. Coast. Conserv.* **1997**, *3*, 57–62. [[CrossRef](#)]
22. Fraser, G.S.; Bennet, S.W.; Olyphant, G.A.; Bauch, N.J.; Ferguson, V.; Gellasch, C.A.; Millard, C.L.; Mueller, B.; O’Malley, P.J.; Way, N.; et al. Windflow circulation patterns in a coastal dune blowout, south coast of Lake Michigan. *J. Coast. Res.* **1998**, *14*, 451–460.
23. Barchyn, T.E.; Hugenholtz, C.H. Reactivation of supply-limited dune fields from blowouts: A conceptual framework for state characterization. *Geomorphology* **2013**, *201*, 172–182. [[CrossRef](#)]
24. Landsberg, H.; Riley, N.A. Wind influences on the transportation of sand over Michigan sand dune. In *Proceedings of the 2nd Hydraulics Conference Bulletin 27*, University of Iowa Studies in Engineering, Iowa City, IA, USA, 1–4 June 1942.
25. Byrne, M.L. Seasonal sand transport through a trough blowout at Pinery Provincial Park, Ontario. *Can. J. Earth Sci.* **1997**, *34*, 1460–1466. [[CrossRef](#)]
26. Jungerius, P.D.; Van Der Meulen, F. Aeolian dynamics in relation to vegetation in a blowout complex in the Meijendel dunes, The Netherlands. *J. Coast. Conserv.* **1997**, *3*, 63–70. [[CrossRef](#)]
27. Hugenholtz, C.H.; Wolfe, S.A. Form-flow interactions of an aeolian saucer blowout. *Earth Surf. Process. Landf.* **2009**, *34*, 919–928. [[CrossRef](#)]
28. Smyth, T.A.G.; Jackson, D.W.T.; Cooper, J.A.G. Computational fluid dynamic modelling of three-dimensional airflow over dune blowouts. *J. Coast. Res.* **2011**, *SI64*, 314–318.
29. Smyth, T.A.G.; Jackson, D.W.T.; Cooper, J.A.G. Three-dimensional airflow patterns within a coastal trough-bowl blowout during fresh breeze to hurricane force winds. *Aeolian Res.* **2013**, *9*, 111–123. [[CrossRef](#)]
30. Smyth, T.A.G.; Jackson, D.W.T.; Cooper, J.A.G. Airflow and aeolian sediment transport patterns within a coastal trough blowout during lateral wind conditions. *Earth Surf. Process. Landf.* **2014**, *39*, 1847–1854. [[CrossRef](#)]
31. Hesp, P.; Walker, I.J. Three-dimensional aeolian dynamics within a bowl blowout during offshore winds: Greenwich Dunes, Prince Edward Island, Canada. *Aeolian Res.* **2012**, *3*, 389–399. [[CrossRef](#)]
32. Puertos del Estado. Available online: <https://www.puertos.es/es-es/oceanografia/Paginas/portus.aspx> (accessed on 25 February 2023).
33. Servera, J. Coastal Dune Systems in Balearic Islands. Ph.D. Thesis, Earth Science Department, University of the Balearic Islands, Mallorca, Spain, 1997. (In Catalan).
34. Roig-Munar, F.X.; Martín-Prieto, J.A.; Rodríguez-Perea, A.; Pons, G.X.; Mir-Gual, M. Risk assessment of beach-dune system erosion: Beach management impacts on the Balearic Islands. *J. Coast. Res.* **2012**, *28*, 1488–1499. [[CrossRef](#)]
35. Folk, R.L.; Ward, W.C. Brazos River bar: A study in the significance of grain size parameters. *J. Sediment. Petrol.* **1957**, *27*, 3–26. [[CrossRef](#)]
36. Jackson, P.S.; Hunt, J.C.R. Turbulent wind flow over a low hill. *Q. J. R. Meteor. Soc.* **1975**, *101*, 929–955. [[CrossRef](#)]
37. Leatherman, S.P. A new aeolian sand trap design. *Sedimentology* **1978**, *25*, 303–306. [[CrossRef](#)]
38. Sarre, R. Eolian sand transport. *Prog. Phys. Geogr.* **1987**, *11*, 155–182. [[CrossRef](#)]
39. Gares, P.A. Topographic changes associated with coastal dune blowouts at Island Beach State Park, NJ. *Earth Surf. Process. Landf.* **1992**, *17*, 589–604. [[CrossRef](#)]
40. Sherman, D.J.; Jackson, D.W.T.; Namikas, S.L.; Wang, J. Wind-blown sand on beaches: An evaluation of models. *Geomorphology* **1998**, *22*, 113–133. [[CrossRef](#)]
41. Sabatier, F.; Chaibi, M.; Pons, F. Validation of aeolian sediment transport formulae by sediment traps. In *Proceedings of the Med & Black Sea Beaches, Sarigerme/Dalaman, Turkey*, 3–27 October 2002.
42. Cabrera, L.L.; Alonso, I. Correlation of aeolian sediment transport measured by sand traps and fluorescent tracers. *J. Mar. Syst.* **2010**, *80*, 235–242. [[CrossRef](#)]

43. Hansen, E.; DeVries-Zimmerman, S.; van Dijk, D.; Yurk, B. Patterns of wind flow and aeolian deposition on a parabolic dune on the southeastern shore of Lake Michigan. *Geomorphology* **2009**, *105*, 147–157. [[CrossRef](#)]
44. Gares, P.A.; Nordstrom, K.F. A cyclic model of foredune blowout evolution for a leeward coast: Island Beach, New Jersey. *Ann. Assoc. Am. Geogr.* **1995**, *85*, 1–20.
45. Jungerius, P.D.; Van Der Meulen, F. The development of dunes blowouts, as measured with erosion pins and sequential air photos. *Catena* **1989**, *16*, 369–376. [[CrossRef](#)]
46. de Rooij, P.C.E.M.; van der Putten, W.H.; Peters, B.A.M. Effects of sand deposition on the interaction between *Ammophila arenaria*, plant-parasitic nematodes, and pathogenic fungi. *Can. J. Bot.* **1995**, *73*, 1141–1150. [[CrossRef](#)]
47. Pethick, J. *An introduction to Coastal Geomorphology*; Edward Arnold Publishers: London, UK, 2001; 272p.
48. Hilton, M. The loss of New Zealand’s active dunes and the spread of marram grass (*Ammophila arenaria*). *N. Z. Geogr.* **2006**, *62*, 105–120. [[CrossRef](#)]
49. Hilton, M.; Konlechner, T. Incipient Foredunes Developed from Marine-dispersed Rhizome of *Ammophila arenaria*. *J. Coast. Res.* **2011**, *SI64*, 288–292.
50. Delgado-Fernandez, I.; Davidson-Arnott, R.G.; Hesp, P.A. Is ‘re-mobilisation’ nature restoration or nature destruction? A commentary. *J. Coast. Conserv.* **2019**, *23*, 1093–1103. [[CrossRef](#)]
51. Walker, I.J.; Davidson-Arnott, R.G.; Bauer, B.O.; Hesp, P.A.; Delgado-Fernandez, I.; Ollerhead, J.; Smyth, T.A. Scale-dependent perspectives on the geomorphology and evolution of beach-dune systems. *Earth-Sci. Rev.* **2017**, *171*, 220–253. [[CrossRef](#)]
52. Arens, S.M.; Van Kaam-Peters, H.M.E.; Van Boxel, J.H. Air flow over foredunes and implications for sand transport. *Earth Surf. Process. Landf.* **1995**, *20*, 315–332. [[CrossRef](#)]

Disclaimer/Publisher’s Note: The statements, opinions and data contained in all publications are solely those of the individual author(s) and contributor(s) and not of MDPI and/or the editor(s). MDPI and/or the editor(s) disclaim responsibility for any injury to people or property resulting from any ideas, methods, instructions or products referred to in the content.